
Q-Mamba: On First Exploration of Vision Mamba for Image Quality Assessment

Fengbin Guan, Xin Li [✉], Zihao Yu, Yiting Lu, and Zhibo Chen [✉]

University of Science and Technology of China

{guanfb,lixin666,yuzihao,luyt31415}@mail.ustc.edu.cn, chenzhibo@ustc.edu.cn

Abstract

In this work, we take the first exploration of the recently popular foundation model, *i.e.*, State Space Model/Mamba, in image quality assessment, aiming at observing and excavating the perception potential in vision Mamba. A series of works on Mamba has shown its significant potential in various fields, *e.g.*, segmentation and classification. However, the perception capability of Mamba has been under-explored. Consequently, we propose Q-Mamba by revisiting and adapting the Mamba model for three crucial IQA tasks, *i.e.*, task-specific, universal, and transferable IQA, which reveals that the Mamba model has obvious advantages compared with existing foundational models, *e.g.*, Swin Transformer, ViT, and CNNs, in terms of perception and computational cost for IQA. To increase the transferability of Q-Mamba, we propose the StylePrompt tuning paradigm, where the basic lightweight mean and variance prompts are injected to assist the task-adaptive transfer learning of pre-trained Q-Mamba for different downstream IQA tasks. Compared with existing prompt tuning strategies, our proposed StylePrompt enables better perception transfer capability with less computational cost. Extensive experiments on multiple synthetic, authentic IQA datasets, and cross IQA datasets have demonstrated the effectiveness of our proposed Q-Mamba.

1 Introduction

Image Quality Assessment (IQA) aims to measure the subjective quality of images aligned with human perception, which has been applied in various visual fields, including visual acquisition, transmission, AIGC [25, 61, 63, 71], and UGC creation [58, 31, 42], etc. Establishing a great IQA metric is necessary to provide the right optimization direction tailored for image processing techniques, *i.e.*, compression [30, 64, 8, 35], enhancement [27, 28, 24, 7], and ensure the perceptual quality of images. Early works on IQA have been achieved by leveraging the natural scene statistics in a hand-crafted manner [44, 46, 60, 52]. With the advancements of deep neural networks (DNNs), learning-based IQA metrics [29, 38, 34, 76, 77, 3] have demonstrated significant potential for low-level perception, which can be roughly categorized into two types based on the pre-trained backbones: CNN-based and Transformer-based methods.

Although the impressive progress, learning-based IQA are susceptible to inherent limitations of existing pre-trained backbones: (i) the CNNs are skilled at learning local translation-invariant features from images while lacking enough long-range dependency modeling capability, hindering the global quality perception. (ii) The emergence of Vision Transformers presents a great solution to model long-range dependency effectively by leveraging attention mechanisms. However, the quadratic complexity of self-attention operations poses unaffordable computational costs, especially for large-scale image quality assessment. Recently, an innovative foundation model, the State Space Model, particularly its implementation, *i.e.*, Mamba [12] has shown considerable potential in various fields for balancing the

[✉] Corresponding authors.

computational costs and performances, *e.g.*, segmentation[65, 43] and classification[54, 80]. This raises one interesting question, *i.e.*, “whether Mamba can surpass existing backbones on low-level visual perception”, which is still under-explored.

To answer this question, in this work, we initiate a new exploration of the Mamba model within the field of image quality assessment (IQA), and introduce the Q-Mamba, a newly developed IQA framework designed to address three key facets of IQA: task-specific, universal, and transferable image quality assessment. Notably, since the lack of enough IQA dataset, learning-based IQA metrics entail the pre-trained backbone for perception knowledge extraction. Meanwhile, VMamba [39], as the most representative framework, has achieved excellent performance on high-level tasks by employing horizontal and vertical scanning strategies. However, merely excavating the global perception knowledge is not optimal for IQA, since most artifacts affecting the image quality are related to local textures. Consequently, inspired by LocalMamba[18], we have adopted a local window scanning method, which significantly enhances Mamba’s ability to perceive local distortions, thereby demonstrating superior performance. We detail the architecture of Q-Mamba and examine different scanning methods to clarify how the model interacts with and processes image data. Our extensive analysis confirms that Q-Mamba surpasses traditional foundational models, showing superior perceptual accuracy and greater computational efficiency.

Moreover, we have explored the perception transferability of Mamba across different datasets, *i.e.*, different contents, and degradations. We can find that the Mamba-based IQA metric still suffers from severe performance drop when they encounter large domain shifts between synthetic distortions[53, 33], authentic distortions[10, 17], and Artificial Intelligence-Generated Content (AIGC)[25, 61] distortions, etc. To further amplify the transferability of Q-Mamba across a range of IQA applications, we introduce a simple but effective tuning strategy called StylePrompt. This is based on the finding that the domain shifts in IQA tend to correlate with their feature statistics/style [41], such as mean and variance. Concretely, our StylePrompt aims to adaptively adjust the mean and variance of pre-trained Q-Mamba towards the target IQA tasks by setting a group of light-weight learnable $1 \times 1 \times C$ parameters. Extensive experiments have shown that our StylePrompt greatly facilitates the task-adaptive learning of Q-Mamba, enabling efficient knowledge transfer across diverse IQA tasks with fewer parameter costs.

The main contributions of this paper are summarized as follows:

- We embark on a novel exploration of the Mamba model within image quality assessment (IQA), and propose the Q-Mamba, a powerful IQA metric for three critical tasks of IQA: task-specific, universal, and transferable image quality assessment. This exploration has demonstrated the superior potential of Mamba for subjective perception, advancing the development of IQA.
- To improve the perception transferability of the Q-Mamba, we introduce a simple but effective tuning strategy, *i.e.*, StylePrompt. This strategy enable the efficient knowledge transfer of pre-trained Q-Mamba for downstream IQA tasks, while only tuning fewer learnable parameters to adjust the statistics of perception features.
- Extensive experiments have shown that our Q-Mamba has consistently achieved state-of-the-art results on various prominent IQA datasets compared with existing IQA methods, thereby validating the efficacy of the Mamba model in quality assessment. Moreover, our StylePrompt achieves nearly equivalent performance to full model tuning while utilizing only 4% of the whole parameters, demonstrating its effectiveness in perception knowledge transfer scenarios.

2 Related Work

2.1 Blind Image Quality Assessment (BIQA)

Early BIQA methods relied heavily on manually designed features for quality score regression [44, 46, 60, 52]. However, these handcrafted features were insufficient for addressing the complexity of BIQA tasks. With the advent of deep learning, network architectures capable of powerful feature extraction significantly improved quality assessment tasks, with Convolutional Neural Networks (CNNs) and Vision Transformers being the most prevalent.

CNN-based BIQA. CNNs have demonstrated robust feature extraction capabilities, leading to their widespread adoption in BIQA tasks. Early works like CNNIQA [20] used convolutional models for feature learning and quality regression, substantially outperforming handcrafted features. DBCNN

[75] introduced a dual-stream network to address synthetic and authentic distortions separately, integrating these insights for better quality prediction. NIMA [57] and PQR [72] leveraged pre-trained models on ImageNet for quality score prediction, enhancing accuracy through well-established neural architectures. MetaIQA [79] employed meta-learning to adapt to unknown distortions by learning shared priors for various distortion types, while HyperIQA [56] used a hypernetwork to adaptively establish perceptual rules, improving generalization. Despite these advancements, CNNs’ local bias limits their ability to fully exploit both global and local information in BIQA tasks.

Transformer-based BIQA. Transformers offer superior global modeling capabilities compared to CNNs. TReS [11] addressed CNNs’ local bias by capturing local structural information with CNNs and then using Transformers for sequential feature extraction. MUSIQ [21] designed a multi-scale image Transformer architecture capable of handling images with varying sizes and aspect ratios. DEIQT [50] leveraged a Transformer-based BIQA architecture with attention mechanisms to align with human perception, enhancing model performance and reducing prediction uncertainty. However, the quadratic complexity of Transformers presents a challenge, highlighting the need for architectures with linear complexity capable of global modeling for BIQA tasks.

2.2 State Space Models (SSMs)

State-space models, known for their linear complexity in capturing long-range dependencies, have been integrated into deep learning architectures. The Structured State-Space model (S4) [14] was a pioneer in deep state-space modeling for remote dependency modeling. Subsequent advancements [13, 55, 9] further propelled the development of state-space models. Mamba [12], by integrating selection mechanisms and hardware-aware algorithms, has shown effective long-range modeling capabilities with linear complexity growth.

Initially focused on NLP tasks, Mamba has rapidly expanded into other domains. Vim [80] introduced a bidirectional SSM block for visual representation learning, achieving performance comparable to ViT [5]. VMamba [39] introduced a cross-scan module to traverse spatial domains and convert non-causal visual images into ordered block sequences, maintaining linear complexity while retaining global receptive fields. LocalMamba [18] employed a window-based scanning approach to integrate local inductive biases, enhancing the visual Mamba model. These advancements validate Mamba’s efficacy in visual tasks, leading to its application in image classification [39, 80, 47, 67, 1], video understanding [62, 4, 26], image restoration [15, 54, 78], point cloud analysis [32, 74, 37], and biomedical image segmentation [43, 65, 51, 36]. This paper explores Mamba’s potential in visual quality perception tasks, providing a simple yet effective baseline for future quality perception research.

3 Method

3.1 Preliminaries

State Space Model (SSM).

Traditional State Space Models (SSMs) utilize first-order differential equations to establish a linear time-invariant system, translating one-dimensional input sequences $x(t) \in \mathbb{R}$ into outputs through hidden states $h(t)$ and $y(t)$, described by:

$$\begin{aligned} h'(t) &= Ah(t) + Bx(t) \\ y(t) &= Ch(t) \end{aligned} \tag{1}$$

For compatibility with deep learning’s sequential input requirements, these models undergo a transition to a discrete framework within the S4 model, using discretization parameters Δ to modify A and B into \bar{A} and \bar{B} :

$$\begin{aligned} h_t &= \bar{A}h_{t-1} + \bar{B}x_t \\ y_t &= Ch_t \end{aligned} \tag{2}$$

$$\begin{aligned} \bar{A} &= \exp(\Delta A) \\ \bar{B} &= (\Delta A)^{-1}(\exp(\Delta A) - I) \cdot \Delta B \end{aligned} \tag{3}$$

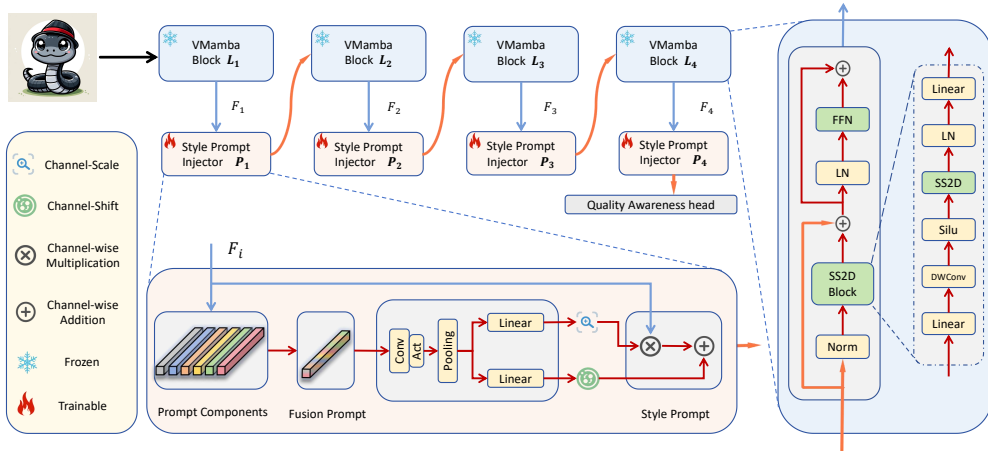


Figure 1: Overview of the Q-Mamba architecture and description of the StylePrompt.

Mamba[12], evolving from these foundations, introduces a selection algorithm for dynamic adaptation of A , B , and C based on input, enhancing model response to complex sequences and contextual variations. However, this necessitates abandoning traditional convolutional methods for kernel fusion and parallel scanning to maintain computational efficiency, effectively scaling with sequence length and providing advanced capabilities in sequence generation for language models.

3.2 Exploring Mamba for Perception

3.2.1 Overall Framework

The overall architecture of our Q-Mamba model is illustrated in Figure 1. To successfully incorporate the Mamba model into visual perception tasks, we implemented the Q-Mamba architecture following the construction method of the VMamba’s visual Mamba blocks. This architecture consists of multiple layers of VMamba blocks, with the SS2D block serving as the core module, which facilitates information transmission through a residual network. The residual network incorporates convolutional layers for feature extraction and activation layers for computing gating signals. We employed multiple network stages, each comprising a downsampling layer and a VMamba Block, which construct multi-level representations at varying resolutions through downsampling, thus extracting richer perceptual features. To explore the impact of model size on quality perception tasks, we experimented with three different scales of the model: QMamba-Tiny, QMamba-Small, and QMamba-Base.

3.2.2 Perception with Local Scanning

Originally, Mamba demonstrated exceptional proficiency in NLP tasks, characterized by inherently causal sequential inputs. However, when adapted to visual tasks, which lack corresponding causal frameworks, the model encountered substantial difficulties. It struggled to effectively discern the complex interdependencies among image pixels, thereby impeding its learning processes.

VMamba[39] employs a novel bidirectional horizontal and vertical scanning mechanism, illustrated in Figure 2(a), to convert two-dimensional data into one-dimensional inputs for model ingestion. Although this method facilitates global modeling of pixel sequences, it unfortunately causes locally adjacent tokens to be spaced significantly apart, thus failing to capture essential local dependencies. This limitation becomes particularly acute in quality assessment tasks, where accurate distortion detection is dependent on the granularity of local detail.

Drawing inspiration from LocalMamba[18], we have implemented a window-based scanning strategy, as depicted in Figure 2(b), to enhance local perceptual accuracy. This involves conducting horizontal scans within each window followed by comprehensive window-level horizontal scans, with a parallel approach adopted in the vertical dimension. This method markedly enhances VMamba’s capability to detect local quality details. Despite the model’s input sequence undergoing downsampling and aggregation, this scanning approach retains an ability for global perception, ensuring a robust

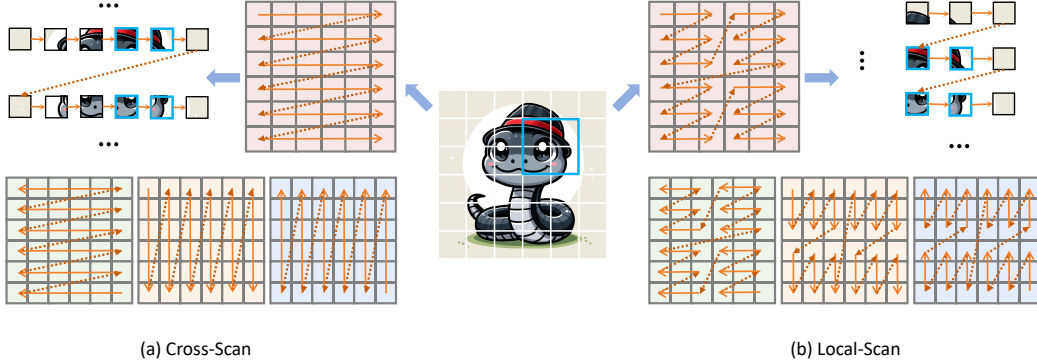


Figure 2: Scanning Methodology Illustration. (a) VMamba’s[39] method flattens 2D data into 1D, impairing connectivity by distancing adjacent tokens. (b) Our local scanning method[18] scans within and across windows, placing semantically similar and distortion-related tokens closer, as shown in the blue boxes.

analytical balance that effectively captures both detailed local nuances and broader contextual information.

3.3 Tuning the Mamba with StylePrompt

Although the Mamba architecture offers reduced computational complexity compared to other models, achieving higher performance still necessitates a substantial number of parameters, which poses a challenge for efficient and transferable learning critical in Image Quality Assessment (IQA) tasks. Prompt tuning[19, 23], a common method for efficient fine-tuning, presents a promising approach. However, conventional prompt tuning techniques involving convolutional or attention operations still require significant parameter overhead[49]. Considering the need for transfer learning in IQA tasks to adapt specifically to the current distortion style, we propose the StylePrompt to enhance the transferability of IQA capabilities. Our method achieves results comparable to full-parameter fine-tuning with a minimal parameter increase. We illustrate the StylePrompt we used in Figure 1. Our StylePrompt consists of two parts, which are described in detail below:

3.3.1 StylePrompt Generation (SPG)

In a multi-stage network architecture, as images progress through each stage of the network, we learn a set of prompts $P_s \in \mathbb{R}^{N \times 1 \times 1 \times C}$, containing N prompt components designed to generate affine parameters for style adaptation. These prompts are specifically utilized to inject the distortion style of the current image into the features $F_i \in \mathbb{R}^{\hat{H} \times \hat{W} \times \hat{C}}$, facilitating learning of the style pertinent to the current domain. We have devised a straightforward StylePrompt Generation stage where the prompt components P_s are initially formed as a set of learnable parameters, interacting with the incoming features to embed distortion information.

To enable the prompt components to extract specific style information from the input stream dynamically, we predict the weights for different prompt components based on the input features. This process involves performing a global pooling on the current layer’s features followed by applying a softmax function to obtain the weights for the prompt group. These weights are then applied to the multiple prompt components to amalgamate them into a new prompt P_f , effectively encapsulating the current style information. The operation can be succinctly summarized by the following formula:

$$P_f = \sum_{c=1}^N w_s P_s, \quad w_s = \text{Softmax}(\text{Conv}1 \times 1(\text{GAP}(F_i))) \quad (4)$$

3.3.2 StylePrompt Injection (SPI)

In the StylePrompt Generation phase, we created the fused prompt P_f , which contains the distortion style information of the current domain. During the StylePrompt Injection process, this style information is injected into the original features $F_i \in \mathbb{R}^{\hat{H} \times \hat{W} \times \hat{C}}$ produced by the current layer. We adapt the distribution of the original features to the style by learning affine parameters. Specifically, as each layer utilizes a fixed-size prompt component, the fused Prompt generated in the StylePrompt Generation phase is matched to the channel dimensions of the current features through linear layers designed to align dimensions. This vector is then processed through two specific linear layers whose primary function is to adjust dimensions, thereby producing the affine parameters $\gamma_v \in \mathbb{R}^{1 \times 1 \times \hat{C}}$ and $\beta_v \in \mathbb{R}^{1 \times 1 \times \hat{C}}$. These parameters are used to inject the distorted style information solely on the channel dimension into the original feature distribution. The process of our StylePrompt Injection can be summarized as follows:

$$\gamma_v = \text{Linear}_\gamma(\text{Conv}(P_f)) \quad (5)$$

$$\beta_v = \text{Linear}_\beta(\text{Conv}(P_f)) \quad (6)$$

$$F'_i = F_i \cdot (1 + \gamma) + \beta \quad (7)$$

Specifically, F'_i represents the original features after the injection of style information. These enhanced features will serve as the new input to the subsequent layer of the network.

4 Experiments

4.1 Experimental Setup

4.1.1 Datasets

We conducted foundational experiments on ten popular IQA datasets, which include four synthetic datasets: LIVE[53], CSIQ[22], TID2013[48], and KADID[33]; four authentic datasets: LIVEC[10], KonIQ[17], LIVEFB[68], and SPAQ[6]; and two AIGC datasets: AIGC2023[61] and AGIQA3K[25]. In our single-task experiments, we utilized all ten datasets for testing. We report the results for the eight datasets consisting of synthetic and authentic datasets in the main text, including comparisons with existing SOTA BIQA methods and performance comparisons of Swin Transformer, ViT, and ResNet across different parameter versions. In the appendix, we report the comparative results of the two AIGC datasets against the aforementioned model architectures. In our universal IQA and transferable IQA experiments, we selected six datasets for training and testing, which include two synthetic datasets (LIVE[53], KADID[33]), two authentic datasets (LIVEC[10], KonIQ[17]), and two AIGC datasets (AIGC2023[61], AGIQA3K[25]).

4.1.2 Evaluation Criteria

The evaluation metrics employed in our study are the widely utilized Pearson Linear Correlation Coefficient (PLCC) and Spearman’s Rank Correlation Coefficient (SRCC), both of which range from 0 to 1. Values approaching 1 denote a higher degree of prediction relevance.

4.1.3 Experimental Details

Our experimental methodology closely adheres to the training strategy outlined in DEIQT[50], where input images are randomly cropped into ten patches of 224×224 resolution. We utilized three variants of the VMamba architecture: VMamba-B, VMamba-S, and VMamba-T. Both VMamba-B and VMamba-S feature an encoder with a depth of 15 layers, where VMamba-B incorporates an embedding dimension of 128, and VMamba-S has an embedding dimension of 96. In contrast, VMamba-T is characterized by a reduced depth of 4 layers and an embedding dimension of 96. Training procedures leveraged weights pre-trained on the ImageNet-1K dataset, spanning across a total of 9 epochs, with batch sizes adjusted according to the respective dataset sizes. All experiments were conducted utilizing multiple NVIDIA RTX 4090 GPUs.

Table 1: Performance comparison for task-specific IQA. Bold indicates the top two results.

Model	LIVE		CSIQ		TID2013		KADID		LIVEC		KonIQ		LIVEFB		SPAQ		Average	
	FLOPs	PLCC	SRCC	PLCC	SRCC	PLCC	SRCC	PLCC	SRCC	PLCC	SRCC	PLCC	SRCC	PLCC	SRCC			
ILNIQE[73]	-	0.906	0.902	0.865	0.822	0.648	0.521	0.558	0.534	0.508	0.508	0.537	0.523	0.332	0.294	0.712	0.713	0.618
BRISQUE[45]	-	0.944	0.929	0.748	0.812	0.571	0.626	0.567	0.528	0.629	0.629	0.685	0.681	0.341	0.303	0.817	0.809	0.664
WaDIQaM[2]	-	0.955	0.960	0.844	0.852	0.855	0.835	0.752	0.739	0.671	0.682	0.807	0.804	0.467	0.455	-	-	0.763
DBCNN[75]	-	0.971	0.968	0.959	0.946	0.865	0.816	0.856	0.851	0.869	0.851	0.884	0.875	0.551	0.545	0.915	0.911	0.852
TIQA[70]	-	0.965	0.949	0.838	0.825	0.858	0.846	0.855	0.850	0.861	0.845	0.903	0.892	0.581	0.541	-	-	0.829
MetalQA[79]	-	0.959	0.960	0.908	0.899	0.868	0.856	0.775	0.762	0.802	0.835	0.856	0.887	0.507	0.540	-	-	0.815
P2P-BM[69]	-	0.958	0.959	0.902	0.899	0.856	0.862	0.849	0.840	0.842	0.844	0.885	0.872	0.598	0.526	-	-	0.835
HyperQA[56]	-	0.966	0.962	0.942	0.923	0.858	0.840	0.845	0.852	0.882	0.859	0.917	0.906	0.602	0.544	0.915	0.911	0.858
TReS[11]	-	0.968	0.969	0.942	0.922	0.883	0.863	0.858	0.859	0.877	0.846	0.928	0.915	0.625	0.554	-	-	0.858
MUSIQ[21]	-	0.911	0.940	0.893	0.871	0.815	0.773	0.872	0.875	0.746	0.702	0.928	0.916	0.661	0.566	0.921	0.918	0.832
DEIQT[50]	-	0.982	0.980	0.963	0.946	0.908	0.892	0.887	0.889	0.894	0.875	0.934	0.921	0.663	0.571	0.923	0.919	0.884
LoDa[66]	-	0.979	0.975	-	-	0.901	0.869	0.936	0.931	0.899	0.876	0.944	0.932	0.679	0.578	0.928	0.925	0.882
ResNet-50(23.51M)	4.11G	0.879	0.884	0.861	0.841	0.747	0.686	0.784	0.786	0.868	0.831	0.908	0.886	0.313	0.269	0.907	0.907	0.772
ResNet-101(42.50M)	7.83G	0.918	0.921	0.891	0.867	0.779	0.727	0.722	0.719	0.862	0.824	0.918	0.904	0.420	0.347	0.908	0.906	0.790
ResNet-152(58.15M)	11.53G	0.926	0.927	0.923	0.899	0.765	0.717	0.764	0.760	0.859	0.816	0.919	0.898	0.433	0.353	0.907	0.907	0.798
ViT-T(5.52M)	1.26G	0.786	0.792	0.725	0.717	0.728	0.699	0.832	0.836	0.777	0.730	0.852	0.852	0.521	0.461	0.896	0.896	0.756
ViT-S(21.67M)	4.61G	0.900	0.896	0.832	0.815	0.873	0.859	0.893	0.894	0.831	0.799	0.922	0.905	0.539	0.443	0.919	0.917	0.827
ViT-B(85.80M)	17.58G	0.961	0.955	0.924	0.912	0.904	0.905	0.910	0.908	0.875	0.837	0.913	0.895	0.491	0.452	0.914	0.912	0.854
Swin-T(27.52M)	4.51G	0.879	0.883	0.865	0.847	0.937	0.925	0.923	0.922	0.880	0.845	0.901	0.881	0.476	0.453	0.922	0.919	0.841
Swin-S(48.84M)	8.77G	0.883	0.896	0.884	0.874	0.931	0.918	0.895	0.894	0.907	0.884	0.931	0.914	0.476	0.433	0.918	0.915	0.847
Swin-B(86.74M)	15.47G	0.945	0.948	0.941	0.935	0.942	0.933	0.934	0.932	0.892	0.858	0.945	0.932	0.507	0.471	0.923	0.921	0.872
QMamba-T(27.99M)	4.47G	0.959	0.959	0.940	0.918	0.951	0.945	0.934	0.930	0.898	0.866	0.941	0.925	0.675	0.581	0.934	0.929	0.893
QMamba-S(49.37M)	8.71G	0.962	0.965	0.921	0.903	0.957	0.955	0.934	0.933	0.903	0.874	0.943	0.930	0.677	0.573	0.932	0.927	0.893
QMamba-B(87.53M)	15.35G	0.960	0.961	0.908	0.889	0.953	0.949	0.935	0.932	0.908	0.876	0.943	0.930	0.675	0.579	0.933	0.929	0.891
LQMamba-T(29.87M)	4.44G	0.958	0.959	0.935	0.916	0.952	0.950	0.938	0.923	0.903	0.863	0.943	0.928	0.672	0.574	0.933	0.927	0.892
LQMamba-S(52.91M)	8.66G	0.962	0.964	0.933	0.914	0.955	0.949	0.941	0.928	0.907	0.882	0.946	0.934	0.676	0.574	0.933	0.929	0.895
LQMamba-B(93.79M)	15.30G	0.959	0.951	0.915	0.889	0.965	0.964	0.943	0.941	0.913	0.888	0.947	0.933	0.675	0.582	0.934	0.929	0.896

4.2 A comparison between different IQA backbones

4.2.1 Task-specific IQA

We conducted comprehensive training and testing across the ten datasets previously introduced, drawing analytical comparisons based on results reported by existing methods. Given the predominance of existing BIQA methods targeting synthetic and distorted datasets, we present in Table 1 a detailed comparative analysis of the performance of state-of-the-art (SOTA) methods alongside popular architectures such as ResNet[16], ViT[5], and Swin Transformer[40], against our Q-Mamba architecture. This comparison elucidates performance discrepancies and computational complexities across different parameter configurations. Our findings demonstrate that the LocalQMamba configuration achieves optimal performance across six datasets and, when juxtaposed with other models of comparable parameter scales, it exhibits lower Gflops, thereby confirming the efficacy and reduced computational complexity of the Mamba architecture. Comparative results for the two AIGC datasets are documented in the appendix in Table 7.

4.2.2 Universal IQA

The efficacy of the Q-Mamba architecture was rigorously assessed across a spectrum of datasets, adopting a joint training protocol on six varied datasets, encompassing two synthetic datasets (LIVE, KADID), two authentic datasets (LIVEC, KonIQ), and two AIGC datasets (AIGC2023, AGIQA3K). Subsequent to this joint training phase, we evaluated the performance outcomes, with the findings depicted in Table 2. These results highlight Q-Mamba’s robust multi-tasking capabilities. In comparison to several established foundational models, Q-Mamba consistently delivered notable performance across the majority of the datasets, thereby substantiating its versatility and effectiveness in managing generalized tasks with high efficacy.

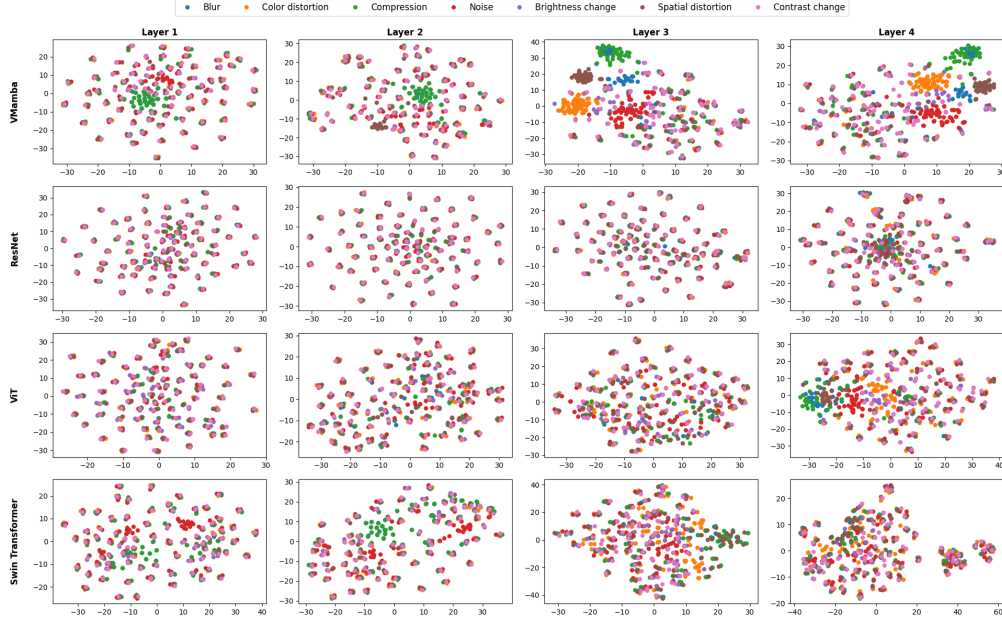


Figure 3: t-SNE clustering of different backbones for various types of distortions

4.2.3 Analysis

To elucidate the reasons behind the VMamba architecture’s notable performance on task-specific IQA and universal IQA tasks, we engaged a subset of the KADID dataset featuring seven distinct types of distortions. We conducted t-SNE[59] dimensionality reduction clustering on the features processed through four disparate model architectures, as illustrated in Figure 3. The clustering outcomes demonstrate that the VMamba architecture exhibits exceptional distortion perception capabilities, effectively distinguishing various types of distortions and surpassing the performance of the ViT structure. Conversely, the ResNet and Swin Transformer architectures did not manifest significant abilities in aggregating different distortion types. Consequently, it becomes apparent that VMamba’s exemplary performance across diverse quality assessment tasks can be attributed, in part, to its robust distortion perception capabilities.

Table 2: Performance comparison for universal IQA. Bold indicates the top two results.

Train		LIVE & KADID & LIVEC & KonIQ & AGIQA3K & AIGCIQA2023												
Test	GFLOPS	LIVE		KADID		LIVEC		KonIQ		AGIQA3K		AIGCIQA2023		Average
		PLCC	SRCC	PLCC	SRCC	PLCC	SRCC	PLCC	SRCC	PLCC	SRCC	PLCC	SRCC	
ResNet-50	4.11G	0.916	0.908	0.868	0.869	0.885	0.841	0.896	0.869	0.884	0.813	0.821	0.815	0.865
ResNet-101	7.83G	0.927	0.921	0.870	0.863	0.885	0.848	0.906	0.878	0.897	0.841	0.843	0.833	0.876
ResNet-152	11.53G	0.936	0.932	0.872	0.866	0.890	0.853	0.911	0.889	0.901	0.841	0.852	0.844	0.882
ViT-T	1.26G	0.878	0.878	0.829	0.828	0.811	0.773	0.824	0.805	0.824	0.745	0.767	0.766	0.811
ViT-S	4.61G	0.921	0.918	0.920	0.917	0.883	0.828	0.911	0.892	0.885	0.822	0.825	0.824	0.879
ViT-B	17.58G	0.941	0.935	0.903	0.901	0.884	0.844	0.912	0.899	0.890	0.826	0.848	0.832	0.885
Swin-T	4.51G	0.927	0.927	0.925	0.921	0.889	0.863	0.929	0.918	0.897	0.840	0.834	0.828	0.892
Swin-S	8.77G	0.946	0.949	0.920	0.916	0.913	0.884	0.929	0.912	0.902	0.844	0.861	0.852	0.902
Swin-B	15.47G	0.945	0.942	0.940	0.937	0.916	0.886	0.940	0.928	0.905	0.847	0.880	0.865	0.911
QMamba-T	4.47G	0.923	0.923	0.938	0.932	0.898	0.863	0.932	0.917	0.906	0.851	0.835	0.830	0.896
QMamba-S	8.71G	0.938	0.941	0.944	0.938	0.905	0.875	0.937	0.923	0.909	0.855	0.853	0.841	0.905
QMamba-B	15.35G	0.922	0.924	0.947	0.942	0.911	0.883	0.939	0.924	0.908	0.857	0.852	0.840	0.904
LQMamba-T	4.44G	0.929	0.926	0.943	0.939	0.899	0.863	0.936	0.921	0.908	0.853	0.840	0.828	0.899
LQMamba-S	8.66G	0.935	0.936	0.942	0.938	0.902	0.870	0.938	0.923	0.912	0.860	0.859	0.843	0.905
LQMamba-B	15.30G	0.941	0.939	0.944	0.941	0.916	0.889	0.939	0.927	0.910	0.859	0.870	0.857	0.911

Table 3: Performance comparison for transferable IQA.

Train	KonIQ & LIVEC								KADID & LIVE								AIGC2023 & AGIQA3K								
Test	KADID		LIVE		AIGC2023		AGIQA3K		KonIQ		LIVEC		AIGC2023		AGIQA3K		KonIQ		LIVEC		KADID		LIVE		
Fine-tuning Method	PLCC	SRCC	PLCC	SRCC	PLCC	SRCC	PLCC	SRCC	PLCC	SRCC	PLCC	SRCC	PLCC	SRCC	PLCC	SRCC	PLCC	SRCC	PLCC	SRCC	PLCC	SRCC	PLCC	SRCC	Average
Without_tuning	0.535	0.501	0.726	0.744	0.789	0.784	0.726	0.744	0.553	0.549	0.595	0.550	0.600	0.612	0.675	0.649	0.636	0.587	0.667	0.637	0.460	0.425	0.815	0.838	0.642
Lin_Probe(R)	0.606	0.581	0.783	0.811	0.824	0.804	0.769	0.695	0.871	0.848	0.785	0.751	0.803	0.788	0.771	0.723	0.818	0.792	0.790	0.761	0.570	0.540	0.799	0.826	0.755
Full_tuning (93.79M)	0.936	0.930	0.941	0.940	0.885	0.863	0.910	0.851	0.943	0.928	0.899	0.873	0.880	0.859	0.910	0.856	0.943	0.927	0.910	0.878	0.937	0.932	0.938	0.933	0.908
StylePrompt (3.83M)	0.920	0.912	0.949	0.948	0.877	0.854	0.908	0.854	0.932	0.913	0.888	0.866	0.880	0.865	0.906	0.852	0.929	0.909	0.902	0.871	0.918	0.913	0.926	0.922	0.901
StylePrompt & R	0.921	0.913	0.944	0.945	0.877	0.853	0.906	0.847	0.931	0.912	0.889	0.860	0.876	0.857	0.905	0.849	0.929	0.909	0.899	0.859	0.918	0.911	0.926	0.927	0.898

4.3 Efficient transfer learning for Mamba-based IQA

In the context of transferable IQA tasks, we engaged in domain-specific training utilizing synthetic datasets (LIVE, KADID), authentic datasets (LIVEC, KonIQ), and AIGC datasets (AIGC2023, AGIQA3K). Each dataset underwent subsequent evaluations in the other two domains. We employed the StylePrompt technique, whereby we maintained the architecture’s integrity during cross-domain transfer by freezing it entirely, and solely fine-tuned the StylePrompt, utilizing merely 4% of the total parameter volume. This approach achieved results that were nearly equivalent to those obtained through full-parameter training. The outcomes, as delineated in Table 3, present a comparative analysis of various fine-tuning strategies, conclusively validating the efficacy and efficiency of our proposed StylePrompt method in facilitating transferable IQA tasks.

4.4 Ablation Studies

4.4.1 Different scanning

Examining the outcomes from task-specific assessment in Table 1 and universal assessment in Table 2, models equipped with local scanning have shown a definitive advantage over those utilizing cross-scanning techniques. This observation has led to an exploration of the effectiveness of local scanning methods.

4.4.2 Different model size

In our empirical analysis, as documented in Table 1 and Table 2, we discern that while QMamba-Base exhibits exceptionally robust quality perception capabilities, QMamba-Small either matches or exceeds the performance of QMamba-Base across the majority of the datasets. Although QMamba-Tiny displays a modest decline in performance metrics, it still delivers results that are competitive with current state-of-the-art (SOTA) methods, solely utilizing the capabilities of QMamba-Tiny.

Table 4: Ablation study on different prompt tuning strategies

Train	KonIQ & LIVEC								KADID & LIVE								AIGC2023 & AGIQA3K								
Test	KADID		LIVE		AIGC2023		AGIQA3K		KonIQ		LIVEC		AIGC2023		AGIQA3K		KonIQ		LIVEC		KADID		LIVE		
Style and Prompt method	PLCC	SRCC	PLCC	SRCC	PLCC	SRCC	PLCC	SRCC	PLCC	SRCC	PLCC	SRCC	PLCC	SRCC	PLCC	SRCC	PLCC	SRCC	PLCC	SRCC	PLCC	SRCC	PLCC	SRCC	Average
SSF(6.1M)	0.718	0.700	0.735	0.769	0.804	0.801	0.714	0.667	0.863	0.829	0.643	0.598	0.668	0.675	0.714	0.685	0.866	0.828	0.730	0.706	0.724	0.708	0.820	0.856	0.743
Crossattn_Prompt(12.17M)	0.843	0.830	0.898	0.897	0.783	0.752	0.821	0.706	0.843	0.816	0.641	0.612	0.802	0.782	0.833	0.726	0.842	0.818	0.644	0.616	0.831	0.815	0.894	0.897	0.789
Conv_Prompt(28.33M)	0.911	0.910	0.945	0.946	0.889	0.820	0.890	0.825	0.897	0.881	0.797	0.761	0.864	0.827	0.861	0.828	0.898	0.884	0.805	0.756	0.901	0.899	0.932	0.933	0.869
StylePrompt(ours)(3.83M)	0.920	0.912	0.949	0.948	0.877	0.854	0.908	0.854	0.932	0.913	0.888	0.866	0.880	0.865	0.906	0.852	0.929	0.909	0.902	0.871	0.918	0.913	0.926	0.922	0.901

4.4.3 Different prompt tuning strategies

To validate the effectiveness of the StylePrompt Generation (SPG) process, we tested the direct learning of a set of affine parameters, γ and β , to modulate the original features. The results in Table 4 demonstrate the outcomes of transfer learning using only the learned affine parameters, substantiating the effectiveness of our StylePrompt Generation phase.

Furthermore, to verify the efficacy of different prompt interaction methods within the StylePrompt, we evaluated various prompt interaction strategies with the original features. These included convolutional prompt interaction and cross-attention prompt interaction. Experimental results indicated

that the interaction method employed by the StylePrompt with the original features achieves the best transfer results with minimal parameter usage. This further validates the effectiveness of our StylePrompt Injection (SPI) phase.

Table 5: Ablation study on the number of prompt

Num of Prompt	PLCC_Average	SRCC_Average	Average
N=1	0.905	0.881	0.8928
N=2	0.905	0.882	0.8936
N=4	0.907	0.884	0.8951
N=6	0.911	0.890	0.9006
N=8	0.905	0.883	0.8939
N=10	0.906	0.883	0.8942

Table 6: Ablation study on the shape of prompts

Prompt_shape(H,W)	PLCC_Average	SRCC_Average	Average
(1,1)	0.911	0.890	0.901
(7,7)	0.909	0.886	0.897
(14,14)	0.909	0.886	0.897
(28,28)	0.907	0.883	0.895
layer_HW	0.908	0.884	0.896

4.4.4 Different Prompt Designs

We investigated the impact of the number of prompt components on performance. Our findings revealed that setting the number of prompts to six yields optimal performance. Furthermore, we explored whether prompts with different spatial dimensions and sizes contribute to enhanced capabilities. Ultimately, we found that a spatial size of (1,1), which solely consists of the channel dimension, yields superior performance. We report the average results of these two ablation studies across multiple datasets in Tables 5 and Table 6. More detailed data will be provided in the appendix Table 8 and Table 9.

5 Conclusion

In this paper, we introduced Q-Mamba, a novel exploration of the Mamba model in the IQA field, which aims to enhance image quality assessment (IQA) from three perspectives: task-specific, universal, and transferable IQA. Our extensive experiments have demonstrated that Q-Mamba has great potential to outperform existing foundational models in IQA, including Swin Transformer, ViT, and CNNs, in both perceptual accuracy and computational efficiency. To improve the perception transferability of Q-Mamba, we developed StylePrompt, a powerful tuning mechanism, to enable the effective perception knowledge transfer of Q-Mamba to various downstream IQA tasks even with large domain shifts, by exploiting only extra 4% of whole parameters to adjust the statistics of perception features of Q-Mamba. We believe these findings can prompt the further development of IQA and pave the way for future research of Mamba-based quality assessment.

References

- [1] A. Behrouz, M. Santacatterina, and R. Zabih. Mambamixer: Efficient selective state space models with dual token and channel selection. *arXiv preprint arXiv:2403.19888*, 2024.
- [2] S. Bosse, D. Maniry, K.-R. Müller, T. Wiegand, and W. Samek. Deep neural networks for no-reference and full-reference image quality assessment. *IEEE Transactions on image processing*, 27(1):206–219, 2017.
- [3] C. Chen, J. Mo, J. Hou, H. Wu, L. Liao, W. Sun, Q. Yan, and W. Lin. Topiq: A top-down approach from semantics to distortions for image quality assessment. *IEEE Transactions on Image Processing*, 2024.
- [4] G. Chen, Y. Huang, J. Xu, B. Pei, Z. Chen, Z. Li, J. Wang, K. Li, T. Lu, and L. Wang. Video mamba suite: State space model as a versatile alternative for video understanding. *arXiv preprint arXiv:2403.09626*, 2024.
- [5] A. Dosovitskiy, L. Beyer, A. Kolesnikov, D. Weissenborn, X. Zhai, T. Unterthiner, M. Dehghani, M. Minderer, G. Heigold, S. Gelly, et al. An image is worth 16x16 words: Transformers for image recognition at scale. *arXiv preprint arXiv:2010.11929*, 2020.
- [6] Y. Fang, H. Zhu, Y. Zeng, K. Ma, and Z. Wang. Perceptual quality assessment of smartphone photography. In *Proceedings of the IEEE/CVF conference on computer vision and pattern recognition*, pages 3677–3686, 2020.
- [7] B. Fei, Z. Lyu, L. Pan, J. Zhang, W. Yang, T. Luo, B. Zhang, and B. Dai. Generative diffusion prior for unified image restoration and enhancement. In *Proceedings of the IEEE/CVF Conference on Computer Vision and Pattern Recognition*, pages 9935–9946, 2023.
- [8] R. Feng, Y. Gao, X. Jin, R. Feng, and Z. Chen. Semantically structured image compression via irregular group-based decoupling. In *Proceedings of the IEEE/CVF International Conference on Computer Vision*, pages 17237–17247, 2023.
- [9] D. Y. Fu, T. Dao, K. K. Saab, A. W. Thomas, A. Rudra, and C. Ré. Hungry hungry hippos: Towards language modeling with state space models. *arXiv preprint arXiv:2212.14052*, 2022.
- [10] D. Ghadiyaram and A. C. Bovik. Massive online crowdsourced study of subjective and objective picture quality. *IEEE Transactions on Image Processing*, 25(1):372–387, 2015.
- [11] S. A. Golestaneh, S. Dadsetan, and K. M. Kitani. No-reference image quality assessment via transformers, relative ranking, and self-consistency. In *Proceedings of the IEEE/CVF winter conference on applications of computer vision*, pages 1220–1230, 2022.
- [12] A. Gu and T. Dao. Mamba: Linear-time sequence modeling with selective state spaces. *arXiv preprint arXiv:2312.00752*, 2023.
- [13] A. Gu, T. Dao, S. Ermon, A. Rudra, and C. Ré. Hippo: Recurrent memory with optimal polynomial projections. *Advances in neural information processing systems*, 33:1474–1487, 2020.
- [14] A. Gu, K. Goel, and C. Ré. Efficiently modeling long sequences with structured state spaces. *arXiv preprint arXiv:2111.00396*, 2021.
- [15] H. Guo, J. Li, T. Dai, Z. Ouyang, X. Ren, and S.-T. Xia. Mambair: A simple baseline for image restoration with state-space model. *arXiv preprint arXiv:2402.15648*, 2024.
- [16] K. He, X. Zhang, S. Ren, and J. Sun. Deep residual learning for image recognition. In *Proceedings of the IEEE conference on computer vision and pattern recognition*, pages 770–778, 2016.
- [17] V. Hosu, H. Lin, T. Sziranyi, and D. Saupe. Koniq-10k: An ecologically valid database for deep learning of blind image quality assessment. *IEEE Transactions on Image Processing*, 29:4041–4056, 2020.

- [18] T. Huang, X. Pei, S. You, F. Wang, C. Qian, and C. Xu. Localmamba: Visual state space model with windowed selective scan. *arXiv preprint arXiv:2403.09338*, 2024.
- [19] M. Jia, L. Tang, B.-C. Chen, C. Cardie, S. Belongie, B. Hariharan, and S.-N. Lim. Visual prompt tuning. In *European Conference on Computer Vision*, pages 709–727. Springer, 2022.
- [20] L. Kang, P. Ye, Y. Li, and D. Doermann. Convolutional neural networks for no-reference image quality assessment. In *Proceedings of the IEEE conference on computer vision and pattern recognition*, pages 1733–1740, 2014.
- [21] J. Ke, Q. Wang, Y. Wang, P. Milanfar, and F. Yang. Musiq: Multi-scale image quality transformer. In *Proceedings of the IEEE/CVF international conference on computer vision*, pages 5148–5157, 2021.
- [22] E. C. Larson and D. M. Chandler. Most apparent distortion: full-reference image quality assessment and the role of strategy. *Journal of electronic imaging*, 19(1):011006–011006, 2010.
- [23] B. Lester, R. Al-Rfou, and N. Constant. The power of scale for parameter-efficient prompt tuning. *arXiv preprint arXiv:2104.08691*, 2021.
- [24] B. Li, X. Li, H. Zhu, Y. Jin, R. Feng, Z. Zhang, and Z. Chen. Sed: Semantic-aware discriminator for image super-resolution. *arXiv preprint arXiv:2402.19387*, 2024.
- [25] C. Li, Z. Zhang, H. Wu, W. Sun, X. Min, X. Liu, G. Zhai, and W. Lin. Agiqa-3k: An open database for ai-generated image quality assessment. *IEEE Transactions on Circuits and Systems for Video Technology*, 2023.
- [26] K. Li, X. Li, Y. Wang, Y. He, Y. Wang, L. Wang, and Y. Qiao. Videomamba: State space model for efficient video understanding. *arXiv preprint arXiv:2403.06977*, 2024.
- [27] X. Li, X. Jin, J. Lin, S. Liu, Y. Wu, T. Yu, W. Zhou, and Z. Chen. Learning disentangled feature representation for hybrid-distorted image restoration. In *Computer Vision—ECCV 2020: 16th European Conference, Glasgow, UK, August 23–28, 2020, Proceedings, Part XXIX 16*, pages 313–329. Springer, 2020.
- [28] X. Li, B. Li, X. Jin, C. Lan, and Z. Chen. Learning distortion invariant representation for image restoration from a causality perspective. In *Proceedings of the IEEE/CVF Conference on Computer Vision and Pattern Recognition*, pages 1714–1724, 2023.
- [29] X. Li, Y. Lu, and Z. Chen. Freqalign: Excavating perception-oriented transferability for blind image quality assessment from a frequency perspective. *IEEE Transactions on Multimedia*, 2023.
- [30] X. Li, J. Shi, and Z. Chen. Task-driven semantic coding via reinforcement learning. *IEEE Transactions on Image Processing*, 30:6307–6320, 2021.
- [31] X. Li, K. Yuan, Y. Pei, Y. Lu, M. Sun, C. Zhou, Z. Chen, R. Timofte, et al. Ntire 2024 challenge on short-form ugc video quality assessment: Methods and results. In *Proceedings of the IEEE/CVF Conference on Computer Vision and Pattern Recognition Workshops*, 2024.
- [32] D. Liang, X. Zhou, X. Wang, X. Zhu, W. Xu, Z. Zou, X. Ye, and X. Bai. Pointmamba: A simple state space model for point cloud analysis. *arXiv preprint arXiv:2402.10739*, 2024.
- [33] H. Lin, V. Hosu, and D. Saupe. Kadid-10k: A large-scale artificially distorted iqa database. In *2019 Eleventh International Conference on Quality of Multimedia Experience (QoMEX)*, pages 1–3. IEEE, 2019.
- [34] J. Liu, X. Li, Y. Peng, T. Yu, and Z. Chen. Swiniqua: Learned swin distance for compressed image quality assessment. In *Proceedings of the IEEE/CVF Conference on computer vision and pattern recognition*, pages 1795–1799, 2022.
- [35] J. Liu, H. Sun, and J. Katto. Learned image compression with mixed transformer-cnn architectures. In *Proceedings of the IEEE/CVF Conference on Computer Vision and Pattern Recognition*, pages 14388–14397, 2023.

- [36] J. Liu, H. Yang, H.-Y. Zhou, Y. Xi, L. Yu, Y. Yu, Y. Liang, G. Shi, S. Zhang, H. Zheng, et al. Swin-umamba: Mamba-based unet with imagenet-based pretraining. *arXiv preprint arXiv:2402.03302*, 2024.
- [37] J. Liu, R. Yu, Y. Wang, Y. Zheng, T. Deng, W. Ye, and H. Wang. Point mamba: A novel point cloud backbone based on state space model with octree-based ordering strategy. *arXiv preprint arXiv:2403.06467*, 2024.
- [38] J. Liu, W. Zhou, X. Li, J. Xu, and Z. Chen. Liqa: Lifelong blind image quality assessment. *IEEE Transactions on Multimedia*, 2022.
- [39] Y. Liu, Y. Tian, Y. Zhao, H. Yu, L. Xie, Y. Wang, Q. Ye, and Y. Liu. Vmamba: Visual state space model. *arXiv preprint arXiv:2401.10166*, 2024.
- [40] Z. Liu, Y. Lin, Y. Cao, H. Hu, Y. Wei, Z. Zhang, S. Lin, and B. Guo. Swin transformer: Hierarchical vision transformer using shifted windows. In *Proceedings of the IEEE/CVF international conference on computer vision*, pages 10012–10022, 2021.
- [41] Y. Lu, X. Li, J. Liu, and Z. Chen. Styleam: Perception-oriented unsupervised domain adaption for non-reference image quality assessment. *arXiv preprint arXiv:2207.14489*, 2022.
- [42] Y. Lu, X. Li, Y. Pei, K. Yuan, Q. Xie, Y. Qu, M. Sun, C. Zhou, and Z. Chen. Kvq: Kwai video quality assessment for short-form videos. *CVPR*, 2024.
- [43] J. Ma, F. Li, and B. Wang. U-mamba: Enhancing long-range dependency for biomedical image segmentation. *arXiv preprint arXiv:2401.04722*, 2024.
- [44] A. Mittal, A. K. Moorthy, and A. C. Bovik. No-reference image quality assessment in the spatial domain. *IEEE Transactions on image processing*, 21(12):4695–4708, 2012.
- [45] A. Mittal, A. K. Moorthy, and A. C. Bovik. No-reference image quality assessment in the spatial domain. *IEEE Transactions on image processing*, 21(12):4695–4708, 2012.
- [46] A. Mittal, R. Soundararajan, and A. C. Bovik. Making a “completely blind” image quality analyzer. *IEEE Signal processing letters*, 20(3):209–212, 2012.
- [47] B. N. Patro and V. S. Agneeswaran. Simba: Simplified mamba-based architecture for vision and multivariate time series. *arXiv preprint arXiv:2403.15360*, 2024.
- [48] N. Ponomarenko, L. Jin, O. Ieremeiev, V. Lukin, K. Egiazarian, J. Astola, B. Vozel, K. Chehdi, M. Carli, F. Battisti, et al. Image database tid2013: Peculiarities, results and perspectives. *Signal processing: Image communication*, 30:57–77, 2015.
- [49] V. Potlapalli, S. W. Zamir, S. Khan, and F. S. Khan. Promptir: Prompting for all-in-one blind image restoration. *arXiv preprint arXiv:2306.13090*, 2023.
- [50] G. Qin, R. Hu, Y. Liu, X. Zheng, H. Liu, X. Li, and Y. Zhang. Data-efficient image quality assessment with attention-panel decoder. In *Proceedings of the AAAI Conference on Artificial Intelligence*, volume 37, pages 2091–2100, 2023.
- [51] J. Ruan and S. Xiang. Vm-unet: Vision mamba unet for medical image segmentation. *arXiv preprint arXiv:2402.02491*, 2024.
- [52] M. A. Saad, A. C. Bovik, and C. Charrier. Blind image quality assessment: A natural scene statistics approach in the dct domain. *IEEE transactions on Image Processing*, 21(8):3339–3352, 2012.
- [53] H. R. Sheikh, M. F. Sabir, and A. C. Bovik. A statistical evaluation of recent full reference image quality assessment algorithms. *IEEE Transactions on image processing*, 15(11):3440–3451, 2006.
- [54] Y. Shi, B. Xia, X. Jin, X. Wang, T. Zhao, X. Xia, X. Xiao, and W. Yang. Vmambair: Visual state space model for image restoration. *arXiv preprint arXiv:2403.11423*, 2024.

- [55] J. T. Smith, A. Warrington, and S. W. Linderman. Simplified state space layers for sequence modeling. *arXiv preprint arXiv:2208.04933*, 2022.
- [56] S. Su, Q. Yan, Y. Zhu, C. Zhang, X. Ge, J. Sun, and Y. Zhang. Blindly assess image quality in the wild guided by a self-adaptive hyper network. In *Proceedings of the IEEE/CVF conference on computer vision and pattern recognition*, pages 3667–3676, 2020.
- [57] H. Talebi and P. Milanfar. Nima: Neural image assessment. *IEEE transactions on image processing*, 27(8):3998–4011, 2018.
- [58] Z. Tu, Y. Wang, N. Birkbeck, B. Adsumilli, and A. C. Bovik. Ugc-vqa: Benchmarking blind video quality assessment for user generated content. *IEEE Transactions on Image Processing*, 30:4449–4464, 2021.
- [59] L. Van der Maaten and G. Hinton. Visualizing data using t-sne. *Journal of machine learning research*, 9(11), 2008.
- [60] N. Venkatanath, D. Praneeth, M. C. Bh, S. S. Channappayya, and S. S. Medasani. Blind image quality evaluation using perception based features. In *2015 twenty first national conference on communications (NCC)*, pages 1–6. IEEE, 2015.
- [61] J. Wang, H. Duan, J. Liu, S. Chen, X. Min, and G. Zhai. Aigciqa2023: A large-scale image quality assessment database for ai generated images: from the perspectives of quality, authenticity and correspondence. In *CAAI International Conference on Artificial Intelligence*, pages 46–57. Springer, 2023.
- [62] J. Wang, W. Zhu, P. Wang, X. Yu, L. Liu, M. Omar, and R. Hamid. Selective structured state-spaces for long-form video understanding. In *Proceedings of the IEEE/CVF Conference on Computer Vision and Pattern Recognition*, pages 6387–6397, 2023.
- [63] X. Wang, X. Li, and Z. Chen. Cono: Consistency noise injection for tuning-free long video diffusion. *arXiv preprint arXiv:2406.05082*, 2024.
- [64] Y. Wu, X. Li, Z. Zhang, X. Jin, and Z. Chen. Learned block-based hybrid image compression. *IEEE Transactions on Circuits and Systems for Video Technology*, 32(6):3978–3990, 2021.
- [65] Z. Xing, T. Ye, Y. Yang, G. Liu, and L. Zhu. Segmamba: Long-range sequential modeling mamba for 3d medical image segmentation. *arXiv preprint arXiv:2401.13560*, 2024.
- [66] K. Xu, L. Liao, J. Xiao, C. Chen, H. Wu, Q. Yan, and W. Lin. Local distortion aware efficient transformer adaptation for image quality assessment. *arXiv preprint arXiv:2308.12001*, 2023.
- [67] C. Yang, Z. Chen, M. Espinosa, L. Ericsson, Z. Wang, J. Liu, and E. J. Crowley. Plainmamba: Improving non-hierarchical mamba in visual recognition. *arXiv preprint arXiv:2403.17695*, 2024.
- [68] Z. Ying, H. Niu, P. Gupta, D. Mahajan, D. Ghadiyaram, and A. Bovik. From patches to pictures (paq-2-piq): Mapping the perceptual space of picture quality. In *Proceedings of the IEEE/CVF conference on computer vision and pattern recognition*, pages 3575–3585, 2020.
- [69] Z. Ying, H. Niu, P. Gupta, D. Mahajan, D. Ghadiyaram, and A. Bovik. From patches to pictures (paq-2-piq): Mapping the perceptual space of picture quality. In *Proceedings of the IEEE/CVF conference on computer vision and pattern recognition*, pages 3575–3585, 2020.
- [70] J. You and J. Korhonen. Transformer for image quality assessment. In *2021 IEEE International Conference on Image Processing (ICIP)*, pages 1389–1393. IEEE, 2021.
- [71] Z. Yu, F. Guan, Y. Lu, X. Li, , and Z. Chen. Sf-iqa: Quality and similarity integration for ai generated image quality assessment. In *Proceedings of the IEEE/CVF Conference on Computer Vision and Pattern Recognition Workshops*, 2024.
- [72] H. Zeng, L. Zhang, and A. C. Bovik. A probabilistic quality representation approach to deep blind image quality prediction. *arXiv preprint arXiv:1708.08190*, 2017.

- [73] L. Zhang, L. Zhang, and A. C. Bovik. A feature-enriched completely blind image quality evaluator. *IEEE Transactions on Image Processing*, 24(8):2579–2591, 2015.
- [74] T. Zhang, X. Li, H. Yuan, S. Ji, and S. Yan. Point could mamba: Point cloud learning via state space model. *arXiv preprint arXiv:2403.00762*, 2024.
- [75] W. Zhang, K. Ma, J. Yan, D. Deng, and Z. Wang. Blind image quality assessment using a deep bilinear convolutional neural network. *IEEE Transactions on Circuits and Systems for Video Technology*, 30(1):36–47, 2020.
- [76] W. Zhang, G. Zhai, Y. Wei, X. Yang, and K. Ma. Blind image quality assessment via vision-language correspondence: A multitask learning perspective. In *Proceedings of the IEEE/CVF conference on computer vision and pattern recognition*, pages 14071–14081, 2023.
- [77] K. Zhao, K. Yuan, M. Sun, M. Li, and X. Wen. Quality-aware pre-trained models for blind image quality assessment. In *Proceedings of the IEEE/CVF Conference on Computer Vision and Pattern Recognition*, pages 22302–22313, 2023.
- [78] Z. Zhen, Y. Hu, and Z. Feng. Freqmamba: Viewing mamba from a frequency perspective for image deraining. *arXiv preprint arXiv:2404.09476*, 2024.
- [79] H. Zhu, L. Li, J. Wu, W. Dong, and G. Shi. Metaiqa: Deep meta-learning for no-reference image quality assessment. In *Proceedings of the IEEE/CVF conference on computer vision and pattern recognition*, pages 14143–14152, 2020.
- [80] L. Zhu, B. Liao, Q. Zhang, X. Wang, W. Liu, and X. Wang. Vision mamba: Efficient visual representation learning with bidirectional state space model. *arXiv preprint arXiv:2401.09417*, 2024.

A Appendix / supplemental material

A.1 Additional experimental results

A.1.1 Task-specific results on AIGCIQA

We present the test results of various backbones on the AIGC datasets in Table 7, with bold indicating the best results.

Table 7: Results of AIGC on various backbones

Model	AGIQA3K		AIGCIQA2023		PLCC_Average	SRCC_Average	Average	
	FLOPs	PLCC	SRCC	PLCC				SRCC
ResNet-50(23.51M)	4.11G	0.901	0.840	0.795	0.797	0.848	0.819	0.833
ResNet-101(42.50M)	7.83G	0.907	0.847	0.834	0.831	0.871	0.839	0.855
ResNet-152(58.15M)	11.53G	0.901	0.832	0.841	0.834	0.871	0.833	0.852
ViT-T(5.52M)	1.26G	0.865	0.787	0.760	0.766	0.813	0.777	0.795
ViT-S(21.67M)	4.61G	0.891	0.819	0.842	0.822	0.867	0.821	0.844
ViT-B(85.80M)	17.58G	0.897	0.830	0.853	0.835	0.875	0.833	0.854
Swin-T(27.52M)	4.51G	0.906	0.847	0.867	0.844	0.887	0.846	0.866
Swin-S(48.84M)	8.77G	0.908	0.849	0.875	0.857	0.892	0.853	0.872
Swin-B(86.74M)	15.47G	0.909	0.852	0.886	0.863	0.898	0.858	0.878
QMamba-T (27.99M)	4.47G	0.913	0.858	0.888	0.873	0.901	0.866	0.883
QMamba-S (49.37M)	8.71G	0.912	0.858	0.889	0.875	0.901	0.867	0.884
QMamba-B (87.53M)	15.35G	0.914	0.861	0.886	0.868	0.900	0.865	0.882
LQMamba-T(29.87M)	4.44G	0.914	0.862	0.884	0.868	0.899	0.865	0.882
LQMamba-S(52.91M)	8.66G	0.913	0.864	0.888	0.869	0.901	0.867	0.884
LQMamba-B(93.79M)	15.30G	0.915	0.858	0.888	0.871	0.902	0.865	0.883

A.1.2 Detailed Results of Ablation Studies

We report the detailed data of our experiments on Prompt design in Table 8 and Table 9.

Table 8: Ablation study results for different numbers of prompts (N).

Train	KonIQ & LIVEC								KADID & LIVE								AIGC2023 & AGIQA3K								Average
	KADID		LIVE		AIGC2023		AGIQA3K		KonIQ		LIVEC		AIGC2023		AGIQA3K		KonIQ		LIVEC		KADID		LIVE		
	PLCC	SRCC	PLCC	SRCC	PLCC	SRCC	PLCC	SRCC	PLCC	SRCC	PLCC	SRCC	PLCC	SRCC	PLCC	SRCC	PLCC	SRCC	PLCC	SRCC	PLCC	SRCC	PLCC	SRCC	
N=1	0.914	0.907	0.943	0.944	0.877	0.850	0.900	0.833	0.924	0.906	0.873	0.846	0.872	0.850	0.898	0.834	0.924	0.907	0.890	0.855	0.904	0.899	0.940	0.937	0.8928
N=2	0.913	0.905	0.938	0.939	0.874	0.851	0.895	0.837	0.930	0.912	0.886	0.853	0.871	0.851	0.892	0.835	0.927	0.905	0.902	0.865	0.911	0.906	0.926	0.922	0.8936
N=4	0.920	0.913	0.944	0.949	0.875	0.851	0.904	0.840	0.929	0.913	0.877	0.849	0.876	0.857	0.904	0.842	0.927	0.904	0.885	0.847	0.913	0.907	0.925	0.931	0.8951
N=6	0.920	0.912	0.949	0.948	0.877	0.854	0.908	0.854	0.932	0.913	0.888	0.866	0.880	0.865	0.906	0.852	0.929	0.909	0.902	0.871	0.918	0.913	0.926	0.922	0.9006
N=8	0.920	0.914	0.930	0.934	0.874	0.851	0.903	0.841	0.930	0.912	0.873	0.843	0.876	0.854	0.899	0.841	0.927	0.906	0.889	0.859	0.918	0.912	0.922	0.926	0.8939
N=10	0.919	0.913	0.930	0.936	0.877	0.856	0.901	0.840	0.929	0.910	0.880	0.849	0.877	0.853	0.900	0.840	0.925	0.906	0.889	0.851	0.918	0.914	0.923	0.924	0.8942

Table 9: Ablation study for different prompt shape

Train	KonIQ & LIVEC								KADID & LIVE								AIGC2023 & AGIQA3K								Average
	KADID		LIVE		AIGC2023		AGIQA3K		KonIQ		LIVEC		AIGC2023		AGIQA3K		KonIQ		LIVEC		KADID		LIVE		
	PLCC	SRCC	PLCC	SRCC	PLCC	SRCC	PLCC	SRCC	PLCC	SRCC	PLCC	SRCC	PLCC	SRCC	PLCC	SRCC	PLCC	SRCC	PLCC	SRCC	PLCC	SRCC	PLCC	SRCC	
(1,1)	0.920	0.912	0.949	0.948	0.877	0.854	0.908	0.854	0.932	0.913	0.888	0.866	0.880	0.865	0.906	0.852	0.929	0.909	0.902	0.871	0.918	0.913	0.926	0.922	0.901
(7,7)	0.924	0.917	0.947	0.948	0.876	0.852	0.906	0.844	0.931	0.912	0.881	0.848	0.875	0.857	0.902	0.843	0.928	0.906	0.890	0.855	0.921	0.915	0.927	0.931	0.897
(14,14)	0.924	0.917	0.947	0.948	0.876	0.852	0.906	0.844	0.931	0.912	0.881	0.848	0.875	0.857	0.902	0.843	0.928	0.906	0.890	0.855	0.921	0.915	0.927	0.931	0.897
(28,28)	0.917	0.909	0.948	0.947	0.871	0.849	0.905	0.847	0.929	0.909	0.876	0.845	0.873	0.855	0.903	0.841	0.928	0.905	0.895	0.860	0.902	0.898	0.932	0.931	0.895
layer_HW	0.921	0.914	0.948	0.948	0.880	0.854	0.905	0.844	0.929	0.909	0.876	0.850	0.879	0.859	0.903	0.844	0.928	0.906	0.891	0.858	0.913	0.908	0.920	0.919	0.896

A.2 Limitations

Q-Mamba heavily relies on pre-trained weights from ImageNet-1K, which may limit its applicability to domains with significantly different data distributions. Future work could explore pre-training on more diverse datasets to improve generalization capabilities. Despite the efficiency improvements brought by the StylePrompt, the computational demands for training and deploying Q-Mamba on very large-scale datasets or in real-time applications might still be substantial. Investigating methods to further reduce computational complexity without sacrificing performance could be beneficial. The current study focuses on specific types of distortions, and there may be other types of distortions that have not been sufficiently explored. Expanding the evaluation to cover a broader range of distortions could provide a more comprehensive validation of Q-Mamba’s robustness. Given that synthetic datasets might not fully capture the complexity and variability of authentic data, there is a risk of overfitting to these synthetic examples. Further evaluations on more diverse and extensive authentic datasets would help ensure the model’s robustness and practical applicability. While Q-Mamba shows promising results in cross-domain transferability, its effectiveness across vastly different domains (e.g., medical imaging versus natural images) has not been thoroughly validated. Further studies are needed to test and possibly adapt Q-Mamba for such diverse applications.

A.3 Broader Impacts

Improving image quality assessment (IQA) through Q-Mamba allows users across various platforms to enjoy higher quality images, enhancing user experience in social media, streaming services, and other digital platforms, thus leading to greater satisfaction and engagement. The enhancement of image quality can significantly benefit individuals with visual impairments, as better image clarity and quality make content more accessible, thereby improving the inclusivity of digital media. Additionally, the computational efficiency of Q-Mamba can result in more efficient image processing workflows, reducing the time and energy required for image enhancement, compression, and transmission. This can lead to cost savings and environmental benefits due to lower energy consumption. Moreover, the transferability of Q-Mamba across different domains can improve image quality in fields such as medical imaging, satellite imagery, and autonomous driving, thereby enhancing the accuracy and reliability of critical applications.

While Q-Mamba presents these positive societal impacts, it is important to acknowledge and mitigate potential negative effects. Enhancing image quality and clarity may inadvertently lead to privacy concerns, as higher quality images can capture more detailed information about individuals and environments. However, our work adheres to ethical guidelines and uses publicly available, open-source datasets, ensuring compliance with various constraints and regulations. By focusing on responsible and ethical use, we aim to maximize the benefits of Q-Mamba while minimizing any adverse societal impacts.